FAKULTA MECHATRONIKY,
INFORMATIKY A MEZIOBOROVÝCH
STUDIÍ TUL

Self-report of the PhD thesis

Fluorescence lifetime imaging via the RATS method in a single-pixel camera configuration

Study program:	P3901 Applied Sciences in Engineering
Field of study:	3901V055 Applied Sciences in Engineering
Author:	**Ing. Jiří Junek**
Supervisor:	doc. RNDr. Karel Žídek, Ph.D.

Liberec 2022

Anotace

Zobrazování doby života fluorescence (FLIM) patří mezi hojně rozšířené přístupy pro analýzu materiálů v široké škále výzkumných témat. Je však vždy nutné zvolit vhodnou principiální metodu pro měření dynamiky fotoluminiscence (PL) vzhledem k měřenému vzorku.

V rámci dizertační práce je představen návrh nové robustní metody, kde není nutná předběžná znalost PL dynamiky vzorku. Princip využívá náhodně modulovaný excitační signál, což umožňuje měřit dohasínání na širokém rozsahu frekvencí v rámci jedné datové sady. To zaručuje přesnou rekonstrukci multi-exponenciální křivky dohasínání PL. Metoda získala název RATS z anglického „Random temporal signals“. Pro účely FLIM lze metodu RATS přenést do 2D snímání například pomocí konfigurace jedno-pixelové kamery (SPC). Zde jsou prezentovány dvě optické uspořádání metody RATS využívající SPC. První z nich využívá dvou difusorů (dvakrát rozptýlené světlo), které jednak zajistí náhodnost časového signálu, ale i náhodné prostorové osvětlení měřeného vzorku -- stěžejní pro rekonstrukci SPC scény. Druhé optické uspořádání je implementace metody RATS do SPC mikroskopu, kde je prostorová náhodnost zajištěna digitálně ovládaným mikro-zrcátkovým čipem (DMD) a časová náhodnost je zajištěn náhodně digitálně modulovaným laserem.

Kromě toho práce představuje dva rekonstrukční přístupy FLIM spektrogramu. První z nich se blíží standardním přístupům rekonstrukce spektrogramu FLIM v SPC. Proto sdílí podobné vlastnosti, jako je počet nutných rekonstrukcí vedoucí k dlouhé době výpočetního zpracování výsledků. Druhý z navrhovaných rekonstrukčních přístupů však potřebuje pouze tolik rekonstrukcí, kolik je dílčích životů dohasínání obsaženo v multi-exponenciální křivce PL dohasínání (obvykle bi-, tri-). To výrazně šetří čas následného zpracování. Navíc umožňuje zobrazení amplitudových map jednotlivých životů PL, což může být přínosné pro výzkum materiálového inženýrství. Oba přístupy jsou analyzovány pomocí simulací z hlediska šumových charakteristik a jsou vzájemně porovnávány.

Nakonec jsou uvedeny myšlenky přímé rekonstrukce parametrů multi-exponenciálních křivek dohasínání v případech se šumem. První návrh, založený na řešení nedourčeného systému, očekává řídké řešení. Poskytuje přesné výsledky, ale není vhodný pro systém se šumem. Druhý návrh, využívá hlubokého učení a ukazuje na možnost získat hledané parametry dohasínání i v systému se šumem. Hladina šumu (0-1%) navíc neovlivňuje přesnost zjištěných parametrů. Tyto přístupy by nahradily regresní zpracování a dále zjednodušily metodu.

Klíčová slova: spektrometrie FLIM, metoda RATS, komprimované snímání, jedno-pixelová kamera

Annotation

Fluorescence lifetime imaging (FLIM) is one of the most widespread approaches to materials analysis in a broad range of scientific fields. However, it is always necessary to choose a principal method for measuring the dynamics of photoluminescence (PL) concerning the measured sample.

As a part of the dissertation thesis, a new robust and straightforward method for PL dynamics measurement is presented, eliminating the need for prior knowledge about the PL dynamics of the sample. The method is based on a randomly modulated excitation signal, which makes it possible to measure PL decay at a wide range of frequencies within a single dataset. This guarantees an accurate reconstruction of the multi-exponential PL decay curve. The method was named RATS according to the "Random temporal signals". The RATS method can be transferred to 2D imaging by using a single-pixel camera (SPC) configuration. Here are presented two optical arrangements of the RATS method in SPC. The first of them is based on two diffusers (double-diffused light), which both ensure the randomness of the temporal signal and the random spatial illumination of the measured sample -- crucial for the SPC scene reconstruction. The second optical arrangement is an implementation of the RATS method into the SPC microscope setup, where spatial randomness is ensured by a digital micro-mirror device (DMD) and temporal randomness is ensured by a randomly digitally modulated laser.

Moreover, two reconstruction approaches for the FLIM spectrogram are introduced. The first of them is close to the standard approaches to FLIM spectrogram reconstruction in SPC and therefore shares similar properties, such as the number of necessary reconstructions leading to the long post-processing time. However, the second of the proposed reconstruction approaches only needs as many reconstructions as the number of partial lifetimes of multi-exponential PL decay (usually bi-, tri-). This significantly saves post-processing time. In addition, it allows displaying the amplitude maps of individual lifetimes, which can be beneficial for material engineering research. Both of them are analyzed via simulations in terms of noise characteristics and are compared.

The thesis is concluded by ideas of precise and direct reconstruction of multi-exponential decay parameters in a noisy system. The first proposed solution, based on an undetermined system, expects a sparse solution. It gives precise results but is not suitable for noisy systems. However, using the second proposal, based on deep learning, it is possible to get precise decay parameters even in noisy systems. Moreover, the noise level (0-1%) does not seriously affect the precision of the found parameters. The algorithms would replace the regression processing and would further simplify the method.

Keywords: FLIM spectrometry, RATS method, compressed sensing, single-pixel camera

Contents

1 Introduction

Due to the ever-evolving research of new materials, optical spectrometry is an essential analytical method, especially because it is a non-destructive and contactless method. One area of spectrometry is focused on photoluminescence (PL) properties. The PL occurs when charged carriers in a material are excited to a higher energy state by a suitable wavelength of photon radiation [1]. The excited carriers spontaneously return to their stable electronic state, partly by generating the above-mentioned PL. The material itself can then be evaluated in terms of the PL wavelength spectrum or studied from the point of view of the PL lifetime, generally referred to as the study of PL dynamics.

The study of PL dynamics thus makes it possible to reveal the lifetimes of PL decay [2] but also deals with the energy levels of charge carriers [3,4] or examines the mechanisms of relaxation and the transfer of excited energy [5,6]. All this information can be obtained for both transparent and non-transparent samples. Therefore, the measurement of PL dynamics is one of the most used characterization methods in the field of chemical physics [7,8], biochemistry [9] but also material sciences in general [10,11].

While the measurement of the time-integrated PL spectrum could be performed using a conventional spectrometer, time-resolved measurement needs advanced optical experimental arrangements, especially for rapid PL decays (nanosecond or sub-nanosecond timescales). Nowadays, there exist several approaches to measuring PL dynamics. Nevertheless, all standard approaches are often based on a pulsed laser, which makes the method expensive. Moreover, we frequently need to have a prior assumption of a measured lifetime. Besides, each method performs best in a limited range of lifetimes [1,12]. Therefore, it is still of great importance to deal with the development of new methods and approaches to measuring PL dynamics.

All these methods can be converted to 2D imaging of PL lifetimes, which is called "Fluorescence Lifetime Imaging" (FLIM) [13]. This approach is used mainly for biological samples (tracing using PL markers), where it is necessary to monitor ongoing processes [14,15]. Therefore, the main development direction is focused on fast data acquisition in terms of the photodegradation of biological samples and PL markers [16,17]. This is aided by a number of approaches, such as avalanche field sensing (SPAD) [18] or the concept of compressed sensing [19]. Besides, an important direction in the field of instrumentation is to create FLIM setups, which are versatile, low-cost and robust with respect to various experimental factors.

This thesis is devoted to the development and optimization of an entirely new approach to the measurement of PL dynamics and FLIM. The novel method - RATS - is proposed as the central part of this work. The method uses a randomly modulated excitation signal for sample excitation, which makes it possible to reconstruct any multi-exponential decay from a single acquired dataset. The method is robust and does not require any signal-timing. For FLIM measurements, the method was implemented in an optical

setup of a single-pixel camera configuration. The thesis comprises all steps, ranging from proof-of-principle experiments, noise analysis, optimization of the method performance with respect to the temporal and spatial resolution, and a novel approach to the analysis of the PL decays in FLIM.

2 Goals definition based on the analysis of the current state-of-the-art

1. Design a robust approach to measuring PL dynamics that eliminates the need for prior knowledge of the PL sample.

   Considering the conclusions of Section 2.1 of the original thesis, it is most often necessary to consider the appropriateness of the given time-resolved method before the actual measurement of the given sample. We also often need to have some prior knowledge about the PL of the sample and set the parameters of the measurement method accordingly. Therefore, finding an approach that eliminates these assumptions would mean a significant simplification of the field.

2. Apply the novel approach to 2D PL lifetime imaging (FLIM) using compressed sensing techniques and define a reconstruction algorithm of the FLIM spectrogram with low post-processing time.

   As stated in the conclusions of Section 2.3 of the original thesis, it is beneficial to substitute a raster mode with an SPC configuration because of shortened measuring time (depending on the compression ratio). However, such an approach suffers from the time cost of post-processing (FLIM spectrogram reconstruction). Therefore, it is advisable to come up with a new solution in the form of an algorithm, where it will not be necessary to reconstruct the entire 3D datacube (x,y,t).

3. Analyze the method in terms of noise dependence and compare the stated reconstruction algorithms of the FLIM spectrogram.

   Noise dependency analysis is a crucial parameter of each method, giving an overview of its utilization. Describe possible ways to suppress noise effect to results and compare stated algorithms of FLIM reconstruction.

4. Analyze the possibility of using the compressed sensing technique to directly determine multi-exponential decay parameters (amplitudes, lifetimes).

   Direct determination of decay parameters would avoid fitting and refine FLIM spectrogram reconstruction. In accordance with the conclusion of Section 2.3 of the original thesis, investigate direct parameters determination using an undetermined system and NN.

3 RATS method

The core of the thesis lies in developing a novel RATS method, which can bypass requirements for advanced optical or electronic setups and represents a robust and low-cost solution.

3.1 Principle of the RATS method

The principle of the RATS method consists of the excitation of the measured sample with a random excitation signal I_{EXC}, which generates a PL signal on the sample, which we designate as I_{PL}. The I_{PL} signal also has a random character because it is given by the convolution of I_{EXC} and I_D according to Eq.(1), where I_D represents the PL decay curve. It is necessary to mention that Eq.(1) is valid only for the PL intensity, which is linearly proportional to the excitation intensity.

$$I_{PL} = I_{EXC} * I_D. \tag{1}$$

Because of using a signal with a random character, we get a wide range of frequencies in Fourier space. Therefore, any multi-exponential I_D can be calculated from a single measured dataset. Eq.(2) shows the deconvolution used with the so-called Tikhonov regularization [44]. The parameter ε controls the ill-conditioned cases where the denominator would approach zero.

$$I_D = Re\left\{ F^{-1}\left[\frac{F\left(I_{PL}\right) F^{*}\left(I_{EXC}\right)}{F\left(I_{EXC}\right)F^{*}\left(I_{EXC}\right) + \varepsilon \overline{F\left(I_{EXC}\right)F^{*}\left(I_{EXC}\right)}} \right] \right\}. \tag{2}$$

The RATS concept can be illustrated by the simulated data shown in Fig. 1. The excitation signal, plotted in blue in Fig. 1(A), was obtained by simulating speckle patterns considering a rotating diffuser using Fraunhofer diffraction [45].

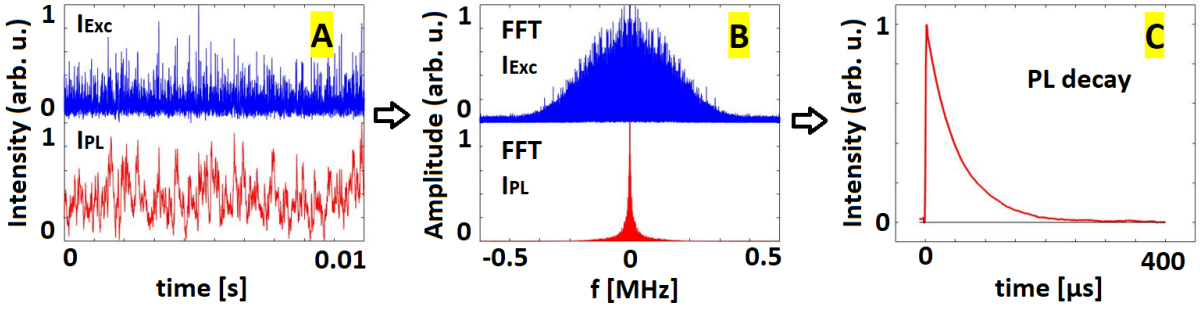

Figure 1: Sequence showing the principle of I_D evaluation by the RATS method. A) Simulated time-modulated I_{EXC} signal (marked in blue) and detected PL signal I_{PL} (marked in red) resulting from mono-exponential decay (τ = 50 µs). B) Fourier transform amplitudes of I_{EXC} (marked in blue) and I_{PL} (marked in red). C) Reconstructed I_D using Eq.(2). Adapted from Junek et al. [47], Fig. 1.

3.2 Random signal generation

3.2.1 Diffuser-based signal generator

One way to generate a random signal is to transmit a coherent beam of light through a rapidly changing scattering element (rotary diffuser).

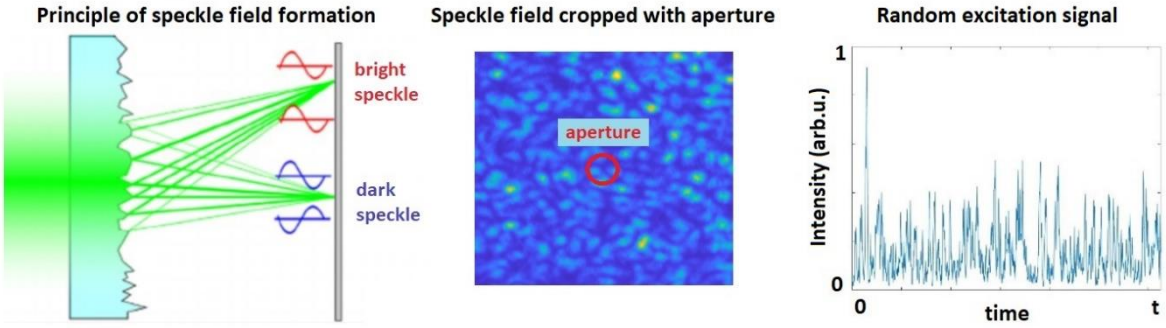

Figure 2: The principle of random signal generation. Left part: An interference speckle pattern formation behind the optical diffusor. Middle part: An example of a speckle pattern with an aperture indicated. Right part: An example of a randomly modulated signal generated by the generator described above.

This approach creates randomly changing interference patterns (see Fig. 2), which we refer to as laser temporal speckles. The field of temporal speckles is cropped by the iris aperture, which gives a random intensity fluctuation in time, which can be used to excite the sample. In the diffuser-based RATS experimental setup, any coherent light source can be used to excite the PL.

3.2.2 Laser modulation-based signal generator

The second way to generate a rapid random signal is using a digital random laser modulation, where a rectangular signal with a random duty cycle is generated. The modulation signal is produced by the development kit Digilent Cmod A7 and was generated in the FPGA Xilinx Artix-7 (VIVADO software package). The bitstream is generated via Linear Feedback Shift Register (LFSR) from flip-flops and XNOR gate feedback, configured in FPGA. The output of the LFSR meets many randomness tests [48].

3.3 Optical setup (0D-RATS)

The RATS method does not require any significantly expensive elements, and due to its simplicity, there is no need for complicated adjustment or calibration of the optical arrangement.

3.3.1 Diffuser signal generator-based optical setup

In general, any coherent light source suitable for sample excitation can be used as the excitation source. An essential part of the optical arrangement is the random signal generator, which consists of three components – a focusing lens, a rotating diffuser, and an aperture.

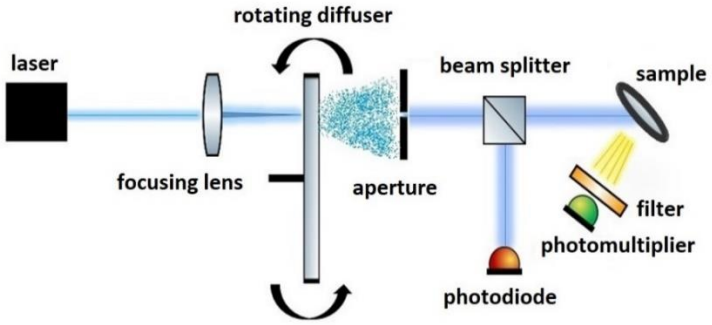

Figure 3: Schematic of the used optical arrangement for single-point 0D-RATS measurement. Adapted from Junek et al. [46], Fig. 2.

The output beam from the generator was divided by a beamsplitter into the reference branch, where the I_{EXC} was detected via a photodiode and transmitted part. The transmitted beam is directed to the measurement branch. A colour filter was used to block the scattered excitation light not to reach the photomultiplier.

3.3.2 Digital signal generator-based optical setup

In the case of using a random digital signal (see Section 3.2.2), the optical setup is significantly simplified, as can be seen from Fig. 4. In addition, the optical power efficiency is increased and depends just on the properties of a used beamsplitter (BS).

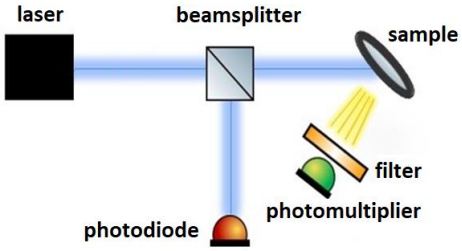

Figure 4: Schematic of 0D-RATS optical setup based on random digital modulation.

3.4 Properties of the RATS method

Due to the use of a random signal, the RATS method can be used to retrieve an arbitrary multi-exponential I_D curve or a non-exponential PL decay.

Both excitation and PL signals (I_{EXC} and I_{PL}, respectively) have to be detected to carry out the reconstruction of PL dynamics. Nevertheless, it is not necessary to attain careful timing of the signals. The mutual temporal shift of the so-called "zero time" between the PL and the excitation data will only cause the decay of the PL to be multiplied by a constant complex number $e^{-i\varphi}$, where the phase φ will be scaled according to the corresponding time difference.

At the same time, the present offset value in the signals (the shift along the *y*-axis) is only reflected at the zero frequency of the Fourier transform and can be avoided by removing low frequencies from the decay reconstruction.

At the same time, the RATS method – as a method based on the deconvolution of a signal – is sensitive to the periodicity of the random excitation signal. From the nature of the deconvolution in Eq.(2), it follows that the periodic waveform leads to a periodic I_D signal with an amplitude distributed between the periodic replica of the PL decay. Therefore, the amplitude of the retrieved PL signal is correspondingly reduced, while the noise present in the data remains the same. Therefore, the approach based on a rotary diffuser can be problematic. However, the periodicity of the excitation signal can be entirely avoided by using a modulated laser (random digital modulation), which can fully replace the analog generator of the random excitation signal (see Section 3.2.2).

3.4.1 Impulse response function

The decisive parameter of PL dynamics spectroscopy is the temporal resolution of the method. This is characterized by the width of the impulse response function (IRF). The IRF in a given optical system can be determined by measuring a sample where the PL decays much faster than the expected IRF width -- the full width at half maximum (FWHM).

I. IRF of the diffuser-based optical setup

In the case of the RATS method, the IRF width is mainly affected by the modulation rate of the I_{EXC} signal, which is related to the speed of temporal fluctuation of the speckles.

In the last experimental campaign, significant progress was achieved towards the optimization of the IRF. The diameter of the focused beam was reduced to 2.3 μm, the measured diameter of the rotating diffuser was 125 mm, the average grain size was around 4 μm and the rotating frequency of the diffuser reached 230 Hz. In such an arrangement, an IRF width = 45 ns was obtained.

II. IRF of the laser modulation-based optical setup

Since the random digital modulation creates a rectangular signal, the signal contains, in addition to the carrier frequency, several significantly higher frequencies related to the steepness of the leading and falling edges. Therefore, when determining the IRF, the sampling frequency played an important role.

The sampling frequency was always chosen to fulfil the Shannon-Nyquist theorem for carrying frequencies of the fastest bit of the signal.

In the best case, we were able to reach the IRF width of 6 ns, which is approximately an order of magnitude improvement compared to the analog mode of temporal speckles generation.

4 2D-RATS

The RATS approach can also be used for 2D fluorescence lifetime imaging (FLIM) via several possible implementations. This thesis was directed towards the single-pixel camera (SPC) configuration, which provides the advantage of the reduced number of measurements. The SPC data can be processed and evaluated via two different approaches, which were introduced in recent manuscripts by Junek et al. [47,49] – see Sections 4.1 and 4.2. Both approaches ($FLIM_B$ and $FLIM_A$) diverge in the steps following Eq.(4).

In the SPC implementation of RATS, the sample is illuminated by a set of random excitation patterns (masks). The intensity of excitation masks fluctuates globally in time so that all pixels are excited with the same temporal waveform $I_{EXC}(t)$. The detected PL intensity corresponds to the sum of PL from all illuminated segments in the sample. Therefore, it can be detected by a single-pixel detector. The I_{PL} signal is then given as the sum of the sub-signals $I_{PL}(i)$ from individual pixels, and Eq.(1) can then be rewritten for the total PL intensity as:

$$I_{PL} = \sum_{i=1}^{n} I_{PL}(i) = I_{EXC} * \sum_{i=1}^{n} I_D(i). \tag{3}$$

The number of excitation masks M is given by the total number of image pixels N and the so-called compression ratio $k = M/N$. Since the masks are not coherent, i.e. they are random to each other, each mask illuminates a different combination of sample segments, and therefore, each individual mask leads to a specific I_{PL} signal. Following the 0D-RATS retrieval of the PL decay, it is possible to extract the PL decay I_{DA} for each mask as:

$$I_{DA} = Re\left\{ \mathbb{F}^{-1}\left[\frac{\mathbb{F}\left(\sum_{i=1}^{n} I_{PL(i)} \right) \mathbb{F}^{*}\left(I_{EXC} \right)}{\mathbb{F}\left(I_{EXC} \right)\mathbb{F}^{*}\left(I_{EXC} \right) + \varepsilon \overline{\mathbb{F}\left(I_{ECX} \right)\mathbb{F}^{*}\left(I_{EXC} \right)}} \right] \right\}. \tag{4}$$

Therefore, we attain M different PL decays I_{DA}, corresponding to M different masks.

4.1 $FLIM_B$ reconstruction approach

As stated in Section 4, the number of calculated PL decay curves I_{DA} corresponds to the number of used masks M. By considering the data from the point of view of mask number, the set of all I_{DA}s provides us with the PL intensity fluctuations at any delay after excitation – see Fig. 5(B). By plotting the intensity fluctuation only at a single delay, we obtain the I_{SPC} signal, where the number of I_{SPC} values corresponds to the number of used masks M (Fig. 5(C)). Using the knowledge of I_{SPC}, the known pattern of the used masks, and compressed sensing algorithms, the PL image $m(t)$ corresponding to the given delay after excitation can be reconstructed. The reconstruction is done via minimization according to Eq.(5).

$$min\left\{\left\|Am(t)-I_{SPC}\right\|_2^2 + TV(m(t))\right\}. \quad (5)$$

The matrix A is created from the vectorized random masks used for the sample excitation. *TV* stands for total variation.

By reconstructing the temporal frame (a 2D image) for each time point of the I_{DA} curve, we obtain a 3D datacube that contains the PL decay curve for each i-th pixel of the $I_D(i,t)$ sample. In each i-th pixel is necessary to perform the fitting to determine the lifetime τ. The whole concept is illustrated and summarized in Fig. 5.

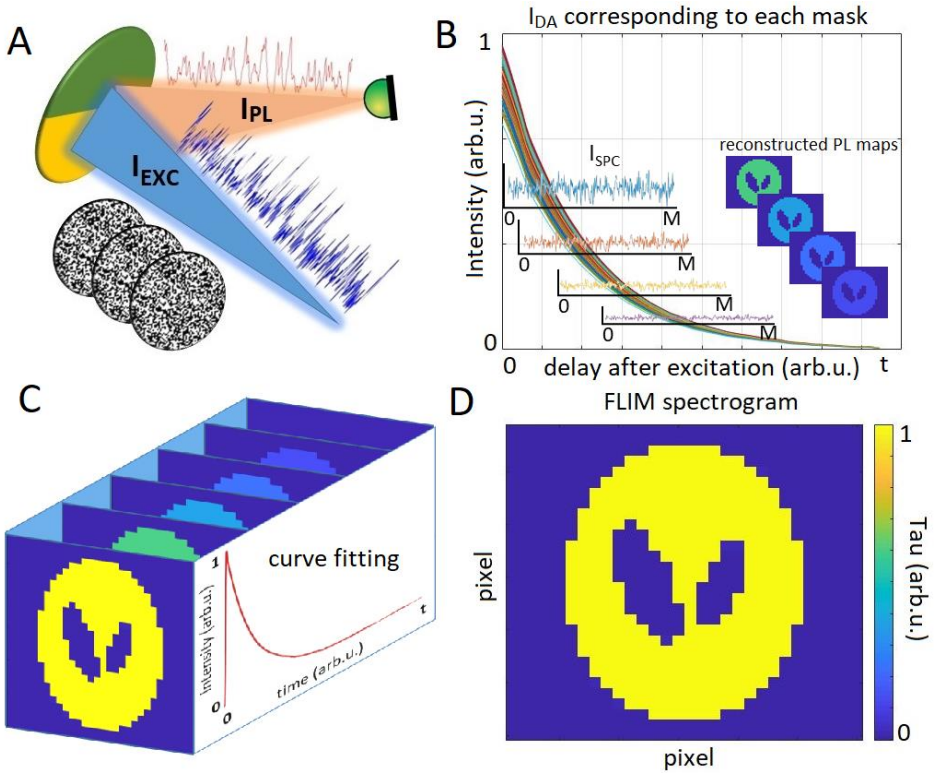

Figure 5: (A)Scheme of the 2D-RATS approach where the sample is illuminated by a set of random patterns (masks) fluctuating in intensity according to $I_{EXC}(t)$. The overall $I_{PL}(t)$ corresponding to the given mask is detected by a single-pixel detector. (B)Example of a set of calculated I_{DA}s for the corresponding set of masks – see Eq.(8) – and fluctuations I_{SPC} in intensity for each delay after excitation. (C)Knowledge of the I_{SPC} signal and the set of used masks will allow determining the PL map m(t) for a given time point t of the I_{DA} curve using reconstruction algorithms. (D)An example of a final FLIM spectrogram as a map of PL lifetimes. Adapted from Junek et al. [49], Fig. 1.

4.2 FLIM$_A$ reconstruction approach

This approach is also based on the use of a single-pixel camera configuration. The assumption is made that if we illuminate the entire measured area with a homogeneous illumination (fluctuating in time according

to I_{EXC}), we can reconstruct the total PL decay curve I_{DA0} according to Eq.(4). The I_{DA0} curve contains all lifetimes τ present in the measured sample, which can be revealed via fitting (so-called zeroth step). The extracted lifetimes then create a cornerstone for the subsequent FLIM data processing. In practice, it is often appropriate to consider a bi-exponential curve, at most a tri-exponential one, mainly because of the similarity of individual multi-exponentials and the possibility of a wrong fit [1]. In the following data processing steps, we will consider a bi-exponential curve (parameters τ_1 and τ_2). Subsequently, the scene is illuminated by a set of *M* masks with *N* pixels -- connected to the compression ratio $k = M/N$. Decay I_{DA}, corresponding to each mask, is determined according to Eq.(4).

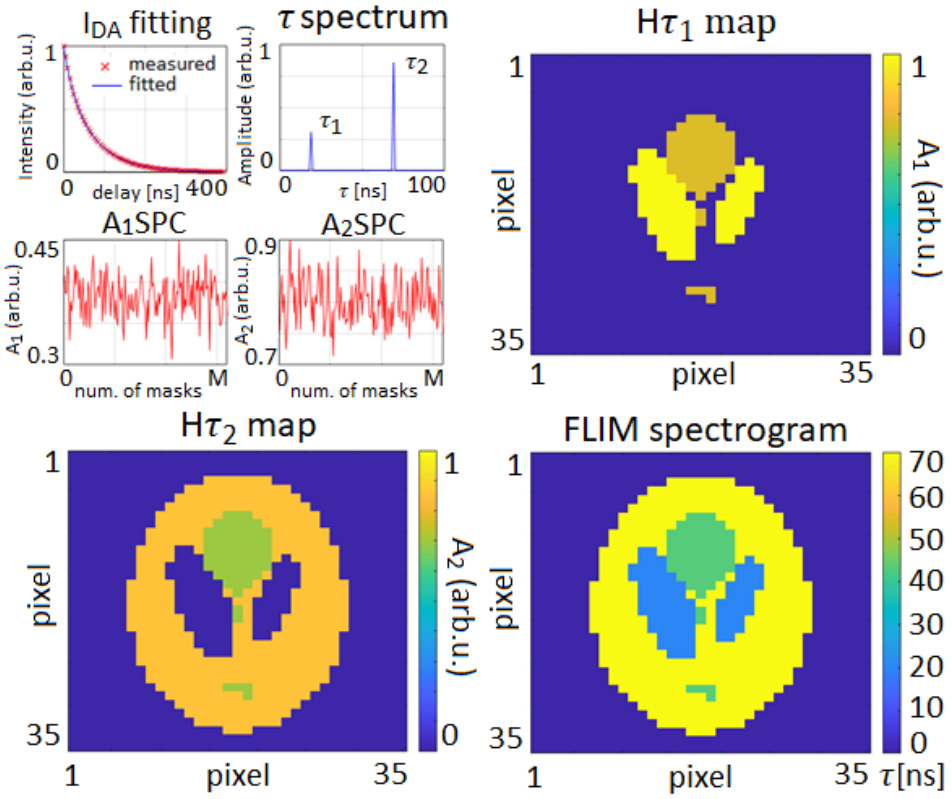

Figure 6: (A) Example of fitting I_{DA} curve amplitudes A_1 and A_2, where the distribution of τ_1 and τ_2 is already known from I_{DA0} fitting. The amplitude fitting provides vectors A_1SPC and A_2SPC. (B) Reconstructed amplitude map $H\tau_1$. (C) Reconstructed amplitude map $H\tau_2$. (D) Calculated FLIM spectrogram based on knowledge of $H\tau_1$ and $H\tau_2$. Adapted from Junek et al. [49]. Fig. 4.

Each I_{DA} is then fitted with the fixed parameters τ_1 and τ_2 -- known from the initial fitting of the total PL decay I_{DA0}. Therefore, the only fitting parameters are A_1 and A_2 (see Eq.(6)). Since the amplitudes connected to the PL lifetimes are extracted for each mask, two vectors, A_1SPC and A_2SPC of size *M*, are obtained. Vectors A_1SPC and A_2SPC contain information about PL amplitude connected to the PL lifetimes τ_1 and τ_2.

$$I_D = A_1 e^{-t/\tau_1} + A_2 e^{-t/\tau_2}. \tag{6}$$

From the knowledge of A_1SPC and A_2SPC and the dataset of random masks B, it is possible to calculate the amplitude maps $H\tau$ corresponding to the individual lifetimes τ_1 and τ_2 according to Eq.(7), where TV denotes the total variation.

$$min\left\{\left\|BH_{\tau n} - A_n SPC\right\|_2^2 + TV(H_{\tau n})\right\}. \tag{7}$$

The lifetime maps can be evaluated individually, and an effective PL lifetime (FLIM spectrogram) is possible to calculate from them. In this thesis, we calculated the desired FLIM spectrogram by the weighted averaging of the present lifetimes. The weights in a given pixel are represented via $H\tau$ maps. In the general case of the n-exponential case, we define the FLIM spectrogram $\tau(x,y)$ as:

$$\tau(x,y) = \frac{\sum_{i=1}^{n} H_{\tau i}\tau_i}{\sum_{i=1}^{n} H_{\tau i}}. \tag{8}$$

The principle of FLIM spectrogram determination using the FLIMA approach is summarized in Fig. 6. We would like to outline a significant reduction of post-processing time -- it is necessary to make only as many reconstructions as the n-exponential case is expected/found.

4.3 Optical setup for 2D-RATS measurement

The optical arrangement of the 2D-RATS depends on the choice of the random signal generator, which was presented in Section 3.2. By choosing an analog signal generator based on a rotary diffuser (see Section 3.2.1), we can expect significant losses in the intensity of the excitation energy compared to a digitally random modulated laser (see Section 3.2.2).

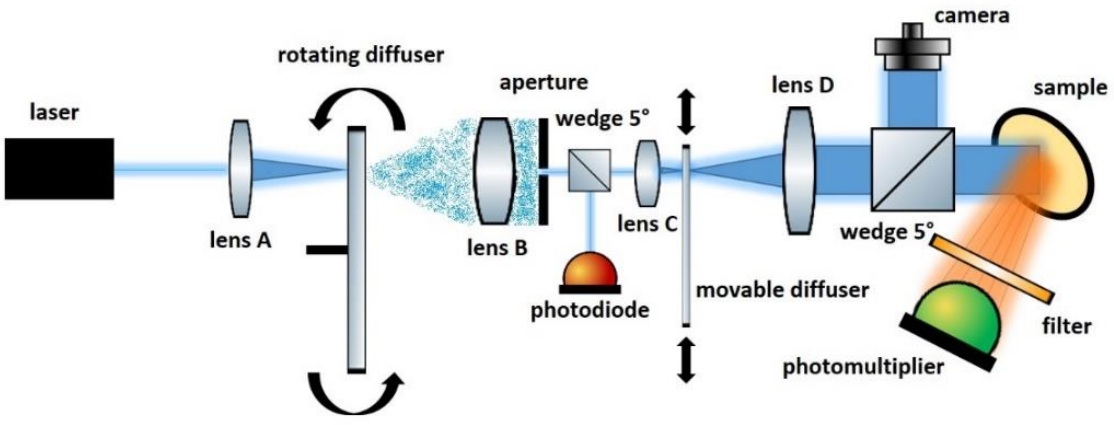

Figure 7: Schematic of the optical arrangement for 2D-RATS in a single-pixel camera configuration based on two optical diffusers. Adapted from Junek et al. [47], Fig. 4.

Another decisive parameter is the approach to random mask generation. The first way is using a laterally sliding diffuser, which can generate masks in grayscale resolution based on the speckle pattern. The second way is using a digital micro-mirror device (DMD) to generate binary masks with the option of choosing a resolution limited by the chip parameters.

Two optical arrangements based on the 2D-RATS method are presented in the thesis. The first one shows the possibility of FLIM measurement using two diffusers (Fig. 7). The second optical setup shows the implementation of the RATS principle into microscopy using DMD and a digitally modulated signal (Fig. 8).

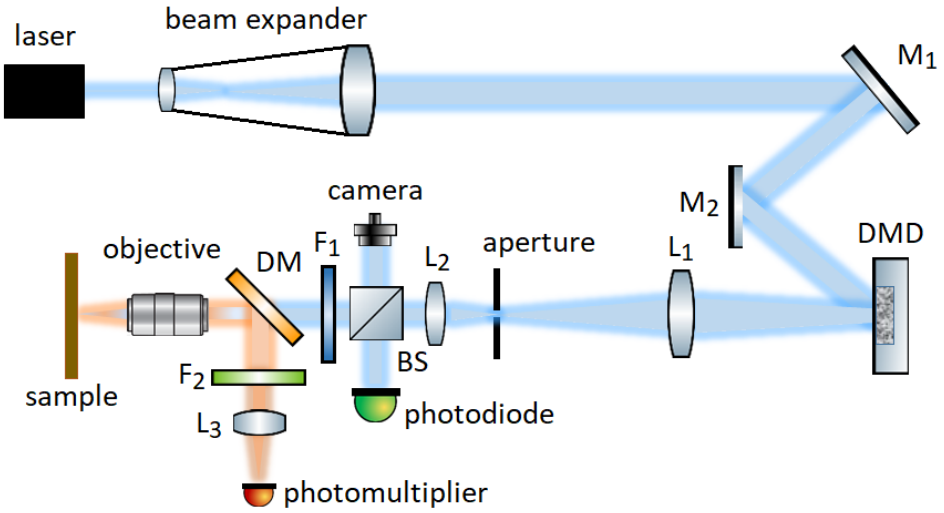

Figure 8: Schematic of a 2D-RATS optical setup implemented in a microscope setup using DMD narrowing and digital time modulation. Adapted from Junek et al. [49], Fig. 7.

4.4 Reconstruction parameters

In both reconstruction approaches, $FLIM_A$ and $FLIM_B$ (see Sections 4.1 and 4.2), we used the TVAL3 algorithm to calculate the undetermined systems [52,53]. The TVAL3 algorithm uses the total variation (*TV*) of reconstructed images as a regularization parameter. The minimization is governed by Eq.(5) or Eq.(7) [54]. The reconstruction parameters were set according to a number of test experiments and simulations. See the original thesis for more details.

4.5 Proof of principle experiments

Several proofs of principle experiments of both reconstruction routines $FLIM_B$ and $FLIM_A$ were performed. However, they are not presented here due to the limited scope of the self-report of the thesis. However, the results can be found in the original thesis or in Junek et al. [47,49].

5 Noise effect analysis

In order to maintain constant conditions, this analysis was performed using simulations that faithfully copied real experimental environments. The primary I_{EXC} signal was simulated using temporal speckle patterns generation [45], considering the realistic random analog signal generator [46]. The analysis showed that the noise added to I_{PL} has a more pronounced effect on reconstructed PL maps than when the noise is added to I_{EXC} (see Fig. 10). It is because the noise distorts reconstructed I_{DA}s (see Fig. 9), so it directly affects the distortion of I_{SPC}.

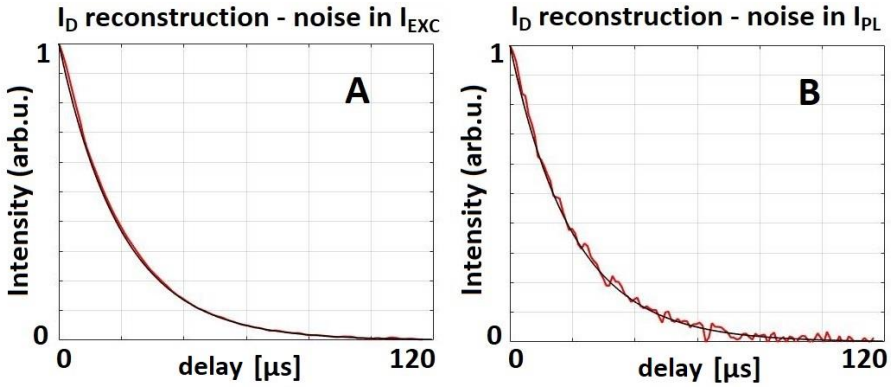

Figure 9: (A) I_D reconstruction with a noise level of 3% in the I_{EXC} signal, corresponding to an SNR of 15.2 dB. I_{PL} was considered noiseless. (B) I_D reconstruction with a noise of 3% in the I_{PL}, corresponding to an SNR of 15.2 dB. I_{EXC} was considered noiseless. Adapted from Junek et al. [50], Fig. 2.

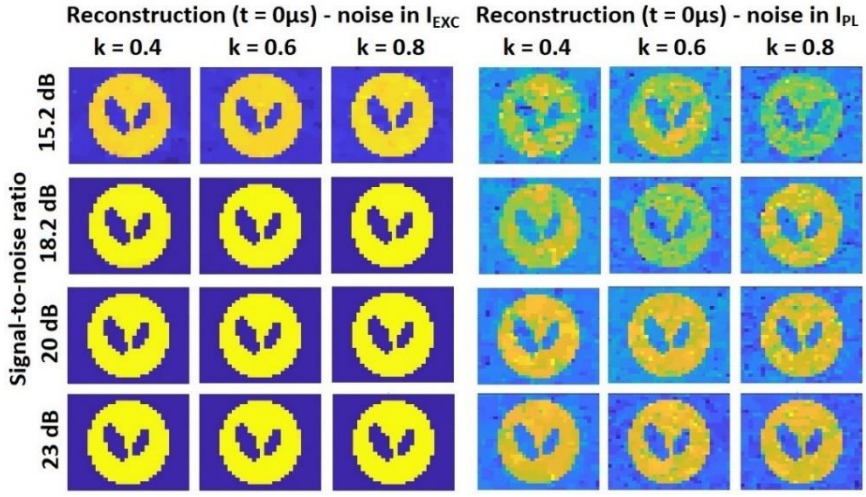

Figure 10: Left part: reconstruction of PL map m(t) at the I_D timepoint of maximal intensity (t = 0 µs) in the case of noise in I_{EXC}. Right part: reconstruction of the PL map m(t) at the timepoint (t = 0 µs) in the case of the noise in the I_{PL}. Rows: signal-to-noise ratios SNR = 15.2, 18.2, 20, 23 dB (rows). Columns: compression ratios k = 0.4, 0.6, 0.8. Adapted from Junek et al. [50], Fig. 3.

Initially, white noise was added only to the I_{EXC} signal, while the I_{PL} signal remained absolutely noiseless and vice versa. The amount of noise added to the system was SNR 23 dB (0.5%), 20 dB (1%), 18.2 dB (1.5%), 15.2 dB (3%), which corresponds to real experimental conditions. The duration of the simulated I_{EXC} signal was 0.1 s with an impulse response function FWHM of 2.07 µs. I_D was considered with τ = 20 µs. The I_{EXC} signal was simulated as non-periodic. Unless otherwise stated further, the regularization parameter ε (see Eq.(2) and Eq.(4)) is kept as ε = 0.1. The result also revealed that it is not easily possible to compensate for the effect of present noise by increasing the compression ratio.

5.1 Optimization of noise effect on PL map reconstruction

It is possible to increase the quality of the acquired I_D or I_{DA} by prolonging the acquisition time. The approach favours the frequencies representing the real signal in the Fourier spectrum and suppresses the artificially added white noise contribution. Since the RATS method is based on signal deconvolution, we used a non-periodic signal I_{EXC} (see Section 3.4). The σ describes the average deviation of reconstructed I_{DREC} and prescripted I_D in all pixels.

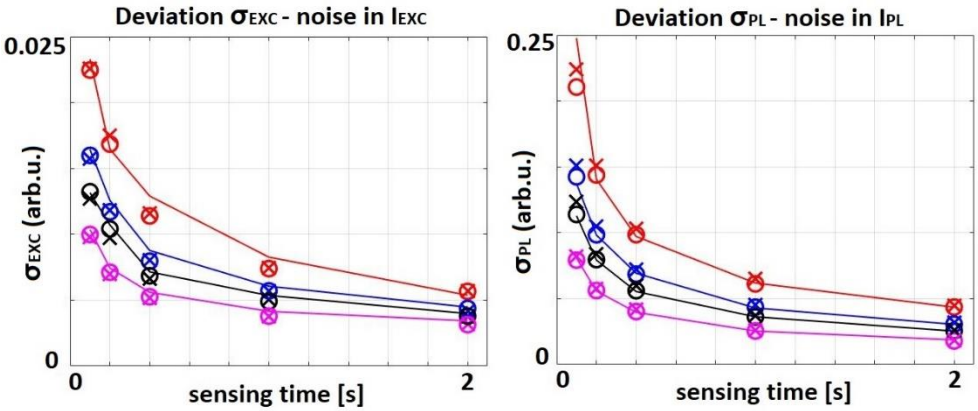

Figure 11: Dependence of the acquisition time on the deviation σ_{EXC} – noise considered in I_{EXC} (left part) and σ_{PL} – noise considered in I_{PL} (right part). SNR: 15.2 dB (red), 18.2 dB (blue), 20 dB (black), 23 dB (magenta) for three different compression ratios k = 0.4 (solid line), k = 0.6 (circle), k = 0.8 (cross). Adapted from Junek et al. [50], Fig. 9.

Another way to eliminate the effect of noise is the choice of the regularization parameter ε in Eq.(2) or Eq.(4). The regularization parameter makes it possible to solve ill-conditioned problems where "division by zero" could occur, i.e. for frequencies with low amplitudes in the I_{EXC} signal [44]. The regularization parameter adds a specific amount of the averaged spectrum power to the denominator (see Eq.(2) and Eq.(4)). Thus eliminating the influence of less frequent frequencies in the signal (white noise). As a result, the calculated I_D or I_{DA} waveform is smoothed.

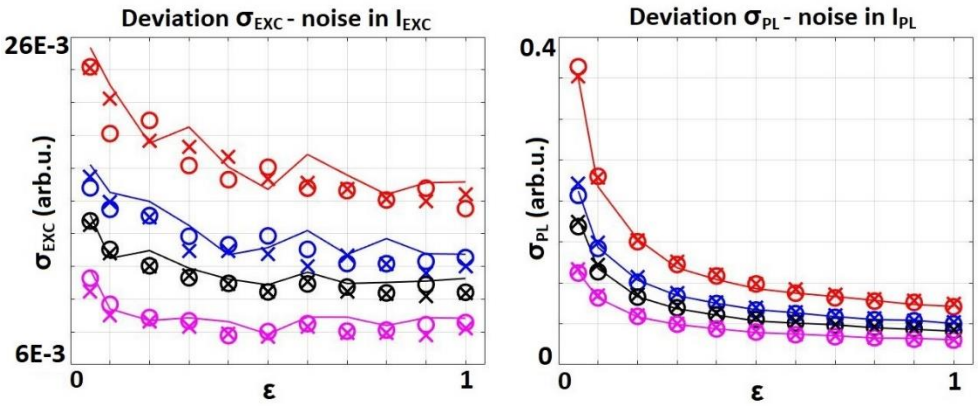

Figure 12: Dependence of ε on deviation σ_{EXC} – noise considered in I_{EXC} (left part) and σ_{PL} – noise considered in I_{PL} (right part). SNR: 15.2 dB (red), 18.2 dB (blue), 20 dB (black), 23 dB (magenta) for three different compression ratios k = 0.4 (solid line), k = 0.6 (circle), k = 0.8 (cross). Adapted from Junek et al. [50], Fig. 12.

Due to the random nature of the signals, no mathematical filtering of the signal was intentionally applied, as important frequencies would easily be eliminated. Mathematical signal filtering could certainly be optimized for one random pattern of signal, but at the expense of the general applicability of the results.

Although the analysis above was made for the $FLIM_B$ approach, most of the knowledge, especially the optimization of the noise effect on the PL decay I_{DA} retrieval for a single random mask I_{DA}, is also freely transferable to the alternative $FLIM_A$ reconstruction approach. The $FLIM_A$ approach is based on the direct reconstruction of amplitude maps corresponding to lifetimes τ (see Section 4.2).

5.2 Noise reconstruction stability of $FLIM_A$ and $FLIM_B$ approaches

Now, we focus directly on the effect of noise on FLIM spectrogram quality, i.e. to compare the precision of the retrieved PL lifetimes in the spectrogram. By doing this, we can compare both approaches, $FLIM_A$ and $FLIM_B$, which feature significantly different data processing.

Based on the results presented in the previous chapters and the results presented by Junek et al. [50], we focused only on the compression ratio $k = 0.4$, and the noise is present only in the measured PL signal I_{PL}, while the excitation dataset I_{EXC} was assumed to be noiseless. The noise level was set to values of 0%, 0.5%, 1%, and 1.5%. The resulting FLIM spectrogram labelled F was evaluated by the percentage deviation R compared to the simulated reference U.

$$R = \frac{\sum \sqrt{(F-U)^2}}{\sum \sqrt{U^2}} \times 100. \tag{9}$$

In view of Fig. 13 and Fig. 14, the $FLIM_A$ approach is more stable in terms of noise, while the $FLIM_B$ approach may experience local errors. Only in the 0% noise case was the $FLIM_B$ approach more

accurate than $FLIM_A$. That is because the overall $FLIM_A$ spectrogram distortion was reflected by a slight deviation in the I_{DA0} fit (so-called zeroth step).

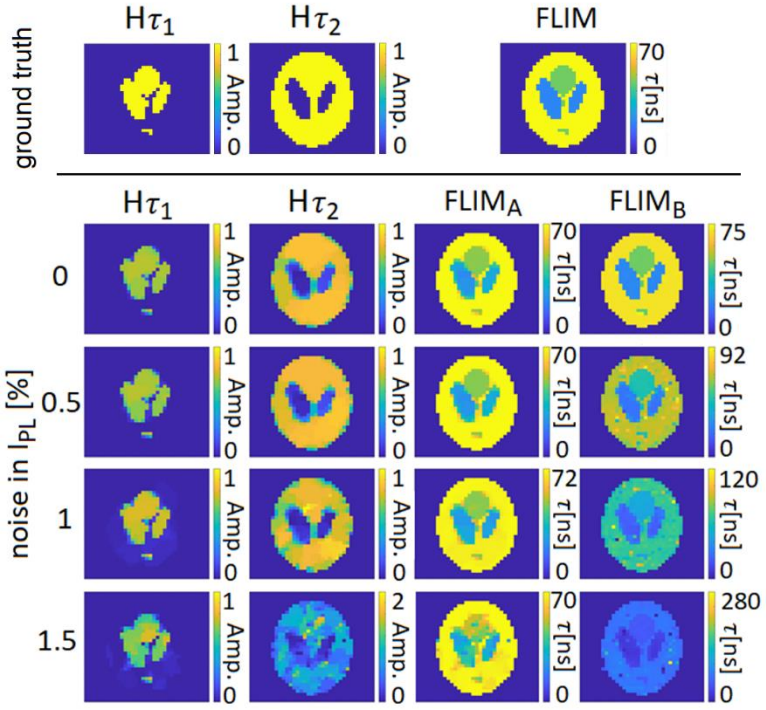

Figure 13: Above the line is the ground truth, which can be compared to the simulated results below the line. The $FLIM_A$ approach is represented in the third column - supplemented by reconstructions of partial amplitude maps $H\tau_1$ (the first column) and $H\tau_2$ (the second column). The results of the $FLIM_B$ approach are presented in the fourth column. Each row corresponds to the chosen noise level in the system (0-1.5%). Adaptet form Junek et. al [49]. Adapted from Junek et al. [49], Fig. 5.

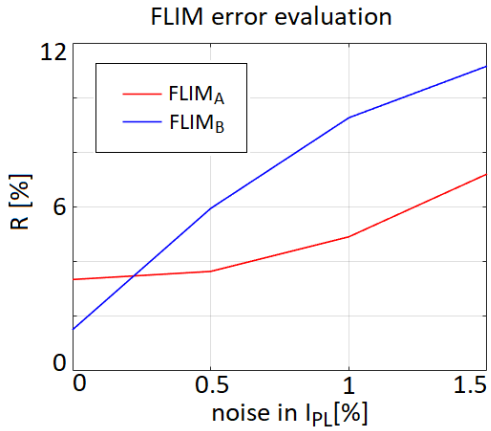

Figure 14: Evaluation of FLIM spectrogram reconstruction error – see Eq.(14) - via $FLIM_A$ (direct PL lifetime map) and $FLIM_B$ (frame-by-frame PL maps reconstruction) approach for a different amount of noise in a system (I_{PL} signal). Adapted from Junek et al. [49], Fig. 6.

6 Direct determination of PL decay parameters

The RATS method can be used to obtain the dynamics of PL decay I_D, which typically has an exponential character in time (mono-exponential, bi-exponential, tri-exponential, …). However, for the sake of data interpretation, the PL lifetime τ needs to be determined. This can only be done during additional data processing, namely by regression of a suitable exponential function. The regression process can be very time-consuming, especially for a 2D scene. Often, it depends on the experimenter which exponential function (mono-, bi-, tri-) is used for regression. Therefore, it is advisable to avoid this step and obtain precise information about the lifetime of PL τ directly from the measured data (random I_{EXC}/I_{PL} signals).

Moreover, it should be kept in mind that in general multi-exponential cases, the shape of the PL decays with two different multi-exponential components can be very similar [58]. Therefore, alternative solutions approaches were investigated using the minimization of the undetermined system or using deep learning.

6.1 Direct determination of decay parameters via an undetermined system

With the assumption of a sparse solution and the vision of the appropriate use of the randomness of the excitation signal, an algorithm was compiled based on the minimization of an undetermined system (described in detail in the original thesis). The algorithm was successfully verified for systems with SNR > 78 dB. However, once we simulate more noisy data, the algorithm fails to converge to the correct result.

The failure of the algorithm with noisy data is apparently caused by the inappropriateness of the measuring matrix *A*, whose randomness is lost due to the character of matrix *B*. In the ideal case of measuring matrix *A*, a completely different I_{EXC} (different *w*) for each τ (column of matrix *B*) should be ensured (see the original thesis). However, this is apparently impossible to ensure in realistic experimentation conditions. Therefore, we turned to a different approach to retrieve the PL lifetimes.

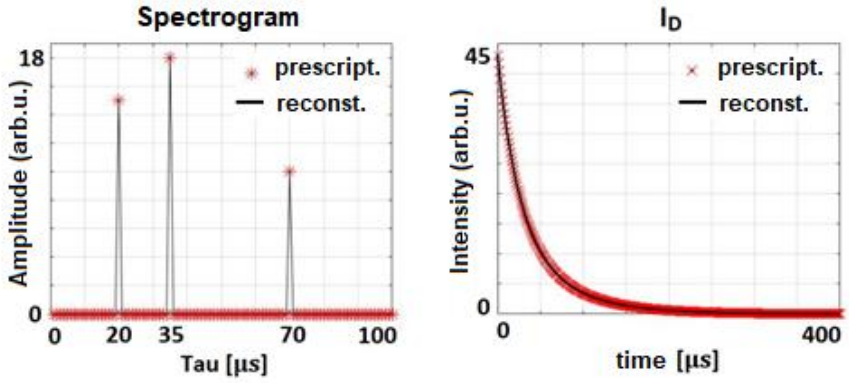

Figure 15: I_D reconstruction consisting of three exponentials with amplitudes - 15, 18, 10 and PL lifetimes τ - 20, 35, 70 µs. Noiseless system.

6.2 Direct determination of PL decay parameters using neural network

The issue of PL lifetime retrieval was also investigated using deep learning and neural networks (NN) as an alternative to the previous algorithms. The problem can be defined as a search for the correct lifetimes from a list of possible options. Therefore, the so-called "multi-task learning" approach was implemented. The multi-task learning is used to recognize multiple objects in the image -- e.g. image analysis used in autonomous vehicles [62].

The training and testing datasets in this subsection are purely synthetic simulated data which reliably copy the real experiment. Data (I_{PL} signals) were generated according to Eq.(1), assuming the same I_{EXC} pattern for all simulations. White noise was added just to the I_{PL} so that the noise level corresponded to a random 1/SNR value selected from intervals 0-1%. In training and testing datasets, we considered only bi-exponential decays, i.e. two present lifetimes τ_1 and $\tau_{2,}$ with a random distribution of amplitudes A_1 and A_2. The training dataset consisted of X = 216 000 simulated traces, where X/6 traces from the data belonged to each investigated lifetime. The same amount of data (X/6) also belonged to the I_{PL} with a different lifetime (6th neuron). The data in the testing dataset was distributed according to the same logic, where the total number of data was Y = 24 000.

Keras and Tensorflow libraries were used to create the NN model based on 1D convolutional neural networks (1D-CNN). For the sake of simplicity and as proof of the principle, the NN was always trained for a set of 5 lifetimes τ, chosen from the interval 1-100 μs. The choice of units does not play here an important role as it can be arbitrarily set in the simulations. The output of NN was 6 neurons. Neurons 1-5 represented the investigated lifetimes, and the sixth neuron represented any other lifetime.

Two cases were explored. In the first case, the training and testing datasets contained closely spaced lifetimes from a selected interval (τ_1 = 20 μs τ_2 = 21 μs τ_3 = 22 μs τ_4 = 23 μs τ_5 = 24 μs). After 20 epochs, NN predicts the complete PL decay lifetime retrieval with an accuracy of 80.5% for the testing set.

In the second case, the datasets contained more distinct lifetimes within the interval 1-100 μs, namely τ_1 = 5 μs τ_2 = 23 μs τ_3 = 40 μs τ_4 = 58 μs τ_5 = 75 μs. After 20 epochs, NN predicts the complete PL decay lifetime retrieval with an accuracy of 81.9% for the testing set.

Due to the facts mentioned in the previous sections, determining adjacent lifetimes (the first case) is a significantly more difficult task in noisy data, and it is often problematic or impossible to solve using commonly used methods [57, 58].

Nevertheless, the results show that the introduced NN solution can provide us with satisfying results. Overall, the results in both training cases (the first case expects close and the second remote lifetimes in the search spectrum) clearly show that by using NN, the accuracy of determining decay lifetimes does not necessarily deteriorate for the noisy cases (tested 0-1%), as it is with standard algorithms.

7 Conclusion

The RATS method was presented as a new method for PL decay measurement, which was fully developed during my Ph.D. study. The method can be used in a single-point measurement (0D-RATS) but also in the imaging mode (2D-RATS), which finds application in fluorescence lifetime imaging (FLIM). The method was successfully verified with the streak camera and TCSPC [46,47].

The demonstration experiments of two implementations of the RATS method were presented in this thesis. In the first implementation, a random excitation signal was generated using a rotary diffuser, and illuminating masks were produced using a laterally moving diffuser (grayscale speckle mask). This implementation is straightforward and incomparably low-cost with respect to standard FLIM approaches. Nevertheless, it is very ineffective in using the excitation light intensity. The second implementation of 2D-RATS was a microscopic setup. It used a DMD to generate illuminating masks (binary masks), and the excitation signal was based on a randomly modulated diode laser. With this approach, it is possible to achieve a temporal resolution in the order of units of a nanosecond and spatial resolution on the micrometer scale.

The thesis also describes two approaches for obtaining a FLIM spectrogram, which we called as $FLIM_A$ and $FLIM_B$. The $FLIM_A$ approach is chronologically younger, and it succeeded in avoiding the need for determining the PL decay curve and lifetime (via fitting) in each pixel separately as in $FLIM_B$. Hence, the post-processing routine is significantly speeded up. In addition, using $FLIM_A$, it is possible to display the amplitude map directly for each partial lifetime, i.e. the distribution of partial lifetimes of multi-exponential decay within the sample.

An important step in the optimization of the RATS method was the analysis of the noise effect on PL data reconstruction. The analysis revealed a significantly higher sensitivity of the results towards the noise corrupting the measured PL signal I_{PL}. In general, the noise level in data turned out to be a key parameter of reconstruction quality, which cannot be effectively compensated by simply increasing the number of measurements, i.e. by increasing the compression ratio.

The simulations showed that an efficient way to significantly increase the signal-to-noise ratio is either a straightforward prolongation of the acquisition time or the possibility of choosing a suitable regularization parameter ε. In the case of prolonging acquisition for one I_{DA} reconstruction, it is necessary to consider a significant increase in the total measurement time. The choice of the regularization parameter ε is related to the noise level in the system since it smoothes the I_D/I_{DA} curve but also causes a slight distortion. Therefore, in situations with low noise, it is convenient to keep the regularization parameter at values $\varepsilon = 0.1$ or $\varepsilon = 0.2$. In the case of higher noises, it is adequate to choose a significantly higher ε. Simulations have shown that with the correct choice of regularization parameter and acquisition time, the

RATS method can achieve results that are not distorted and can accurately map a 2D scene even with a relatively high noise level (3%).

The periodicity of the excitation signal I_{EXC} was discussed as part of the noise analysis. The attained data showed that periodicity decreases the signal-to-noise ratio. This issue arises due to the application of the deconvolution step in the PL decay retrieval. Since the original means of generation of the random signal was based on a rotating diffuser, the periodicity effect could play a significant role. Therefore, we replaced the original method with a randomly modulated laser with a random seed, which became a cornerstone of the so-called second generation of the 2D-RATS setup. Direct laser modulation turned out to be a better solution for the RATS systems.

Most of the insights gathered through the detailed noise analysis could be applied to both $FLIM_A$ and $FLIM_B$ reconstruction approaches. Although $FLIM_A$ and $FLIM_B$ are different, it is necessary to reconstruct the PL decay curve in both cases. The two different approaches to data treatment were compared through their FLIM spectrograms for noise levels of 0-1.5%. The $FLIM_A$ approach showed more accurate results in situations with higher noise levels than 0%.

Finally, we pursued the idea of creating an algorithm for the direct reconstruction of the PL decay parameters with the assumption of an undetermined system. The algorithm searched for a sparse solution and worked successfully in noiseless systems. However, in a situation with SNR < 78 dB, the algorithm failed to converge to correct results due to the similarity of the different multi-exponential decays.

Therefore, the possibility of using neural networks (NN) with a multi-task learning approach was investigated. The NN model was built on a 1D convolutional neural network (CNN), assuming a limited number of searched lifetimes τ, noise presence from 0-1%, and considering only a bi-exponential decay system. Considering the difficulty of the issue, NN shows high accuracy in precise determining of PL decay curve. In addition, on the tested area of noise (0-1%), the results did not show any significant dependence on the accuracy of lifetime determination with respect to arising noise level. These findings would be beneficial for a wide range of other disciplines of spectrometry, where the exponential fitting is a fundamental part of the analysis, including, for instance, cavity ring-down spectrometry [66,67].

Overall, the thesis presents a novel robust time-resolved method RATS for studying PL dynamics. The method can be easily implemented into a FLIM measurement based on SPC configuration. In the search for a noise-resistant FLIM analysis, we developed two reconstruction strategies, where the direct extraction of decay lifetimes shows better noise stability and significantly reduces post-processing time. We verified that using trained NN, it is possible to determine the lifetime distribution of the bi-exponential system without the result being significantly affected by the amount of present noise (0-1%).

Reference

[1] I. Pelant and J. Valenta, *Luminescence Spectroscopy of Semiconductors* (Oxford University, 2012).

[2] R. M. Clegg and P. C. Schneider, "Fluorescence Lifetime-Resolved Imaging Microscopy: A General Description of Lifetime-Resolved Imaging Measurements," in *Fluorescence Microscopy and Fluorescent Probes*, J. Slavík, ed. (Springer, US, 1996).

[3] L. Foglia, S. Vempati, B. Tanda Bonkano, L. Gierster, M. Wolf, S. Sadofev, and J. Stähler, "Revealing the competing contributions of charge carriers, excitons, and defects to the non-equilibrium optical properties of ZnO," Struct. Dyn. **6**(3), 034501 (2019).

[4] K. Žídek, F. Trojánek, P. Malý, L. Ondič, I. Pelant, K. Dohnalová, L. Šiller, R. Little, and B. R. Horrocks, "Femtosecond luminescence spectroscopy of core states in silicon nanocrystals," Opt. Express **18**(24), 25241–25249 (2010).

[5] A. Lavie-Cambot, C. Lincheneau, M. Cantuel, Y. Leydet, and N. D. McClenaghan, "Reversible electronic energy transfer: a means to govern excited-state properties of supramolecular systems," Chem. Soc. Rev. **39**(2), 506–515 (2010).

[6] K. Kůsová, O. Cibulka, K. Dohnalová, I. Pelant, J. Valenta, A. Fučíková, K. Žídek, J. Lang, J. Englich, P. Matějka, P. Štěpánek, and S. Bakardjieva, "Brightly Luminescent Organically Capped Silicon Nanocrystals Fabricated at Room Temperature and Atmospheric Pressure," ACS Nano **4**(8), 4495–4504 (2010).

[7] A. Fojtik and A. Henglein, "Surface Chemistry of Luminescent Colloidal Silicon Nanoparticles," J. Phys. Chem. B **110**(5), 1994–1998 (2006).

[8] K. Zheng, K. Žídek, M. Abdellah, M. E. Messing, M. J. Al-Marri, and T. Pullerits, "Trap States and Their Dynamics in Organometal Halide Perovskite Nanoparticles and Bulk Crystals," J. Phys. Chem. C **120**(5), 3077–3084 (2016).

[9] P. I. H. Bastiaens and A. Squire, "Fluorescence lifetime imaging microscopy: spatial resolution of biochemical processes in the cell," Trends Cell Biol. **9**(2), 48–52 (1999).

[10] J. M. Griffin, A. J. Miller, A. J. Berry, S. Wimperis, and S. E. Ashbrook, "Dynamics on the microsecond timescale in hydrous silicates studied by solid-state 2H NMR spectroscopy," Phys. Chem. Chem. Phys. **12**(12), 2989–2998 (2010).

[11] K. Dohnalová, L. Ondič, K. Kůsová, I. Pelant, J. L. Rehspringer, and R.-R. Mafouana, "White-emitting oxidized silicon nanocrystals: Discontinuity in spectral development with reducing size," J. Appl. Phys. **107**(5), 053102 (2010).

[12] D. Lin and W. Ma, "Single molecule fluorescence imaging within living cells," PHYSICS-BEIJING- **36**, 783 (2007).

[13] W. Becker, "Fluorescence lifetime imaging – techniques and applications," Journal of Microscopy **247**, 119–136 (2012).

[14] J. A. Levitt, D. R. Matthews, S. M. Ameer-Beg, and K. Suhling, "Fluorescence lifetime and polarization-resolved imaging in cell biology," Current Opinion in Biotechnology **20**, 28–36 (2009).

[15] Q. Wu, J. Qi, D. Lin, W. Yan, R. Hu, X. Peng, and J. Qu, "Simultaneous acquisition of trajectory and fluorescence lifetime of moving single particles," in *Multiphoton Microscopy in the Biomedical Sciences XVII* (SPIE, 2017), **10069**, 269–273.

[16] P. Knotek, L. Tichy, D. Arsova, Z. G. Ivanova, and H. Ticha, "Irreversible photobleaching, photorefraction and photoexpansion in GeS2 amorphous film," Materials Chemistry and Physics **119**, 315–318 (2010).

[17] X. Liu, D. Lin, W. Becker, J. Niu, B. Yu, L. Liu, and J. Qu, "Fast fluorescence lifetime imaging techniques: A review on challenge and development," J. Innov. Opt. Health Sci. **12**, 1930003 (2019).

[18] N. Krstajić, S. Poland, J. Levitt, R. Walker, A. Erdogan, S. Ameer-Beg, and R. K. Henderson, "0.5 billion events per second time correlated single photon counting using CMOS SPAD arrays," Opt. Lett., OL **40**, 4305–4308 (2015).

[19] J. V. Thompson, J. D. Mason, H. T. Beier, and J. N. Bixler, "High speed fluorescence imaging with compressed ultrafast photography," in *High-Speed Biomedical Imaging and Spectroscopy: Toward Big Data Instrumentation and Management II* (SPIE, 2017), **10076**, 74–79.

[20] J. Sytsma, J. M. Vroom, D. Grauw, and H. C. Gerritsen, "Time-gated fluorescence lifetime imaging and microvolume spectroscopy using two-photon excitation," J. Microsc. **191**(1), 39–51 (2008).

[21] R. V. Krishnan, H. Saitoh, H. Terada, V. E. Centonze, and B. Herman, "Development of a multiphoton fluorescence lifetime imaging microscopy system using a streak camera," Rev. Sci. Instrum. **74**(5), 2714–2721 (2003).

[22] S. Cheng, R. M. Cuenca, B. Liu, B. H. Malik, J. M. Jabbour, K. C. Maitland, J. Wright, Y.-S. L. Cheng, and J. A. Jo, "Handheld multispectral fluorescence lifetime imaging system for in vivo applications," Biomed. Opt. Express **5**(3), 921–931 (2014).

[23] A. D. Elder, C. F. Kaminski, and J. H. Frank, "ϕ^2FLIM: a technique for alias-free frequency domain fluorescence lifetime imaging," Opt. Express **17**(25), 23181–23203 (2009).

[24] W. Becker, A. Bergmann, G. Biscotti, K. Koenig, I. Riemann, L. Kelbauskas, and C. Biskup, "High-speed FLIM data acquisition by time-correlated single-photon counting," Proc. SPIE **5323**, 27–35 (2004).

[25] N. Krstajić, S. Poland, J. Levitt, R. Walker, A. Erdogan, S. Ameer-Beg, and R. K. Henderson, "0.5 billion events per second time correlated single photon counting using CMOS SPAD arrays," Opt. Lett. **40**(18), 4305–4308 (2015).

[26] E. P. Buurman, R. Sanders, A. Draaijer, H. C. Gerritsen, J. J. F. van Veen, P. M. Houpt, and Y. K. Levine, "Fluorescence lifetime imaging using a confocal laser scanning microscope," Scanning **14**, 155–159 (1992).

[27] R. V. Krishnan, H. Saitoh, H. Terada, V. E. Centonze, and B. Herman, "Development of a multiphoton fluorescence lifetime imaging microscopy system using a streak camera," Review of Scientific Instruments **74**, 2714–2721 (2003).

[28] S. Cheng, R. M. Cuenca, B. Liu, B. H. Malik, J. M. Jabbour, K. C. Maitland, J. Wright, Y.-S. L. Cheng, and J. A. Jo, "Handheld multispectral fluorescence lifetime imaging system for in vivo applications," Biomed. Opt. Express, BOE **5**, 921–931 (2014).

[29] C. Huber, I. Klimant, C. Krause, and O. S. Wolfbeis, "Dual Lifetime Referencing as Applied to a Chloride Optical Sensor," Anal. Chem. **73**, 2097–2103 (2001)

[30] R. Tibshirani, "Regression Shrinkage and Selection Via the Lasso," Journal of the Royal Statistical Society: Series B (Methodological) **58**, 267–288 (1996).

[31] S. G. Mallat and Z. Zhang, "Matching pursuits with time-frequency dictionaries," IEEE Transactions on Signal Processing **41**, 3397–3415 (1993).

[32] P. L. Combettes and J.-C. Pesquet, "Proximal Splitting Methods in Signal Processing," in *Fixed-Point Algorithms for Inverse Problems in Science and Engineering*, H. H. Bauschke, R. S. Burachik, P. L. Combettes, V. Elser, D. R. Luke, and H. Wolkowicz, eds., Springer Optimization and Its Applications (Springer, 2011), pp. 185–212.

[33] P. Sen, B. Chen, G. Garg, S. R. Marschner, M. Horowitz, M. Levoy, and H. P. A. Lensch, "Dual photography," in *ACM SIGGRAPH 2005 Papers*, SIGGRAPH '05 (Association for Computing Machinery, 2005), pp. 745–755.

[34] G. M. Gibson, G. M. Gibson, S. D. Johnson, S. D. Johnson, M. J. Padgett, and M. J. Padgett, "Single-pixel imaging 12 years on: a review," Opt. Express, OE **28**, 28190–28208 (2020).
[35] Don and M. L, *Designing for Compressive Sensing: Compressive Art, Camouflage, Fonts, and Quick Response Codes* (US Army Research Laboratory, 2018).
[36] V. Studer, J. Bobin, M. Chahid, H. S. Mousavi, E. Candes, and M. Dahan, "Compressive fluorescence microscopy for biological and hyperspectral imaging," Proc. Natl. Acad. Sci. U. S. A. **109**(26), E1679–E1687 (2012).
[37] Q. Pian, R. Yao, N. Sinsuebphon, and X. Intes, "Compressive hyperspectral time-resolved wide-field fluorescence lifetime imaging," Nat. Photonics **11**(7), 411–414 (2017).
[38] R. Yao, M. Ochoa, P. Yan, and X. Intes, "Net-FLICS: fast quantitative wide-field fluorescence lifetime imaging with compressed sensing – a deep learning approach," Light Sci Appl **8**, 26 (2019).
[39] L. Gao, J. Liang, C. Li, *W. Lihong, "*Single-shot compressed ultrafast photography at one hundred billion frames per second". Nature **516**, 74–77 (2014).
[40] J. V. Thompson, J. D. Mason, H. T. Beier, and J. N. Bixler, "High speed fluorescence imaging with compressed ultrafast photography," in *High-Speed Biomedical Imaging and Spectroscopy: Toward Big Data Instrumentation and Management II* (SPIE, 2017), **10076**, 74–79.
[41] S. Yang, J. Lee, Y. Lee, M. Lee, and B.-U. Lee, "Estimation of multiexponential fluorescence decay parameters using compressive sensing," JBO **20**, 096003 (2015).
[42] V. Zickus, M.-L. Wu, K. Morimoto, V. Kapitany, A. Fatima, A. Turpin, R. Insall, J. Whitelaw, L. Machesky, C. Bruschini, D. Faccio, and E. Charbon, "Fluorescence lifetime imaging with a megapixel SPAD camera and neural network lifetime estimation," Sci Rep **10**, 20986 (2020).
[43] J. T. Smith, R. Yao, N. Sinsuebphon, A. Rudkouskaya, N. Un, J. Mazurkiewicz, M. Barroso, P. Yan, and X. Intes, "Fast fit-free analysis of fluorescence lifetime imaging via deep learning," Proceedings of the National Academy of Sciences **116**, 24019–24030 (2019).
[44] A. N. Tikhonov and V. Y. Arsenin, "Solutions of ill-posed problems," SIAM Rev. **21**, 266–267 (1977).
[45] F. Gascón and F. Salazar, "A simple method to simulate diffraction and speckle patterns with a PC," Optik **117**(2), 49–57 (2006).
[46] J. Junek, L. Ondič, and K. Žídek, "Random temporal laser speckles for the robust measurement of sub-microsecond photoluminescence decay," Opt. Express, OE **28**, 12363–12372 (2020).
[47] J. Junek, and K. Žídek, "Fluorescence lifetime imaging via spatio-temporal speckle patterns in a single-pixel camera configuration," Opt. Express, OE **29**, 5538–5551 (2021).
[48] G. Marsaglia, "Xorshift RNGs," Journal of Statistical Software 8, 1–6 (2003).
[49] J. Junek and K. Žídek, " Nanosecond compressive fluorescence lifetime microscopy imaging via the RATS method with a direct reconstruction of lifetime maps," arXiv: 2208.13640 [physics] (2022).
[50] J. Junek, and K. Žídek, "Noise effect on 2D photoluminescence decay analysis using the RATS method in a single-pixel camera configuration," Opt. Express 30(8), 12654–12669 (2022).
[51] K. A. Selanger, J. Falnes, and T. Sikkeland, "Fluorescence lifetime studies of Rhodamine 6G in methanol," J. Phys. Chem. **81**(20), 1960–1963 (1977).
[52] C. Li, Wotao Yin, and Yin Zhang, TVAL3 Home, Rice University, 2009, Last updated 11/07/2013, (available from: https://www.caam.rice.edu/∼optimization/L1/TVAL3/).
[53] C. Li, W. Yin, and Y. Zhang, "User's guide for TVAL3: TV minimization by augmented lagrangian and alternating direction algorithms," CAAM Rep.20, 46–47 (2009).
[54] C. Li, "An Efficient Algorithm For Total Variation Regularization with Applications to the Single Pixel Camera and Compressive Sensing," Master Thesis, Rice University (2009).
[55] Yu. Zorenko, V. Gorbenko, A. Voloshinovskii, G. Stryganyuk, V. Mikhailin, V. Kolobanov, D. Spassky, M. Nikl, and K. Blazek, "Exciton-related luminescence in LuAG:Ce single crystals and single crystalline films," physica status solidi (a) 202, 1113–1119 (2005).
[56] M. Nikl, "Energy transfer phenomena in the luminescence of wide band-gap scintillators," physica status solidi (a) 202, 201–206 (2005).
[57] A. A. Istratov and O. F. Vyvenko, "Exponential analysis in physical phenomena," Review of Scientific Instruments 70, 1233–1257 (1999)
[58] J. R. Lakowicz, *Principles of Fluorescence Spectroscopy* (Springer US, 1983).
[59] T. Blumensath and M. Davies, "On the difference between orthogonal matching pursuit and orthogonal least squares," (2007).
[60] D. Needell and R. Vershynin, "Signal Recovery From Incomplete and Inaccurate Measurements Via Regularized Orthogonal Matching Pursuit," IEEE Journal of Selected Topics in Signal Processing **4**, 310–316 (2010).
[61] Orthogonal Least Squares Algorithms for Sparse Signal Reconstruction [Accessed 25 January 2021]. Available from: [online].
[62] S. Chowdhuri, T. Pankaj, and K. Zipser, "MultiNet: Multi-Modal Multi-Task Learning for Autonomous Driving," in *2019 IEEE Winter Conference on Applications of Computer Vision (WACV)* (2019), pp. 1496–1504.
[63] Baldi and P. J. Sadowski, "Understanding Dropout," in *Advances in Neural Information Processing Systems* (Curran Associates, Inc., 2013), Vol. 26.
[64] M. Li, T. Zhang, Y. Chen, and A. J. Smola, "Efficient mini-batch training for stochastic optimization," in Proceedings of the 20th ACM SIGKDD International Conference on Knowledge Discovery and Data Mining, KDD '14 (Association for Computing Machinery, 2014), pp. 661–670.
[65] D. P. Kingma and J. Ba, "Adam: A Method for Stochastic Optimization," in (2014).
[66] K. Lehmann, "An Introduction to Cavity Ring-Down Spectroscopy," Cavity Ring-Down Spectroscopy (2009).
[67] H. Zu, B. Li, Y. Han, and L. Gao, "Combined cavity ring-down and spectrophotometry for measuring reflectance of optical laser components," Opt. Express, OE **21**, 26735–26741 (2013).

List of all author’s publications

1. J. Junek, and K. Žídek, "Luminescence Decay Measurement via Temporal Speckles," in *Imaging and Applied Optics 2019 (COSI, IS, MATH, PcAOP) (2019), Paper CW4A.7* (Optical Society of America, 2019), p. CW4A.7. (**author's contribution:** 70%)

2. J. Junek, L. Ondič, and K. Žídek, "Random temporal laser speckles for the robust measurement of sub-microsecond photoluminescence decay," Opt. Express, OE **28**(8), 12363–12372 (2020). (**author's contribution:** 60%)

3. J. Junek, and K. Zidek, "FLIM via RATS Method Using Single Pixel Camera," in *Imaging and Applied Optics Congress (2020), Paper JW5C.1* (Optical Society of America, 2020), p. JW5C.1. (**author's contribution:** 70%)

4. J. Junek, and K. Žídek, "Fluorescence lifetime imaging via spatio-temporal speckle patterns in a single-pixel camera configuration," Opt. Express, OE **29**(4), 5538–5551 (2021). (**author's contribution:** 70%)

5. J. Junek, and K. Žídek, "Noise Effect to Data Acquisition Time in FLIM via RATS Method Using Single-Pixel Camera Configuration," in *OSA Optical Sensors and Sensing Congress 2021 (AIS, FTS, HISE, SENSORS, ES) (2021), Paper JTh6A.8* (Optical Society of America, 2021), p. JTh6A.8. (**author's contribution:** 70%)

6. J. Junek, and K. Žídek, "Noise effect on 2D photoluminescence decay analysis using the RATS method in a single-pixel camera configuration," Opt. Express, OE **30**(8), 12654–12669 (2022). (**author's contribution:** 70%)

7. P. Reinig, H.-G. Dallmann, M. Schwarzenberg, J. Ziebarth, J. Knobbe, J. Junek, R. Herbst, J. Rathert, R. Gerlach, U. Blache, S. Tretbar, and S. Fricke, "MEMS-based confocal laser scanning fluorescence microscopy for tumor demarcation in oncological surgery," in Advanced Biomedical and Clinical Diagnostic and Surgical Guidance Systems XX (SPIE, 2022), Vol. 11949, pp. 32–40. (**author's contribution:** 8%)

8. J. Junek and K. Žídek, "Nanosecond compressive fluorescence lifetime microscopy imaging via the RATS method with a direct reconstruction of lifetime maps," arXiv: 2208.13640v3 [physics] (2022). (**author's contribution:** 80%)

Author's publications with scope outside of the thesis

9. J. Budasz, J. Junek, and J. Václavík, "Broadband antireflective coating for NEOSTED," in *Optics and Measurement International Conference 2016* (SPIE, 2016), Vol. 10151, pp. 213–221. (**author's contribution:** 30%)

10. Junek J, "Model mechanického napětí v systému multivrstev," Jemná mechanika a optika, **63**(2), 62-64 (2018). (**author's contribution:** 100%)

11. Špína M., Procháska F., Junek J., Malá K, "Analýza referenčních povrchových vad optických ploch za použití konfokální mikroskopie, interferometrie v bílém světle a mikroskopie atomárních sil," Jemná mechanika a optika **63**(3), 81-84 (2018). (**author's contribution:** 10%)

12. Junek J., Šulc M, "Měření intenzity světla koherentních svazků pod úrovní šumu detektoru," Jemná mechanika a optika **64**(1), 20-23 (2019). (**author's contribution:** 70%)

List of included publications in the thesis

[A] J. Junek, L. Ondič, and K. Žídek, "Random temporal laser speckles for the robust measurement of sub-microsecond photoluminescence decay," Opt. Express, OE **28**(8), 12363–12372 (2020).

[B] J. Junek, and K. Žídek, "Fluorescence lifetime imaging via spatio-temporal speckle patterns in a single-pixel camera configuration," Opt. Express, OE **29**(4), 5538–5551 (2021).

[C] J. Junek, and K. Žídek, "Noise effect on 2D photoluminescence decay analysis using the RATS method in a single-pixel camera configuration," Opt. Express, OE **30**(8), 12654–12669 (2022).

[D] J. Junek and K. Žídek, "Nanosecond compressive fluorescence lifetime microscopy imaging via the RATS method with a direct reconstruction of lifetime maps," arXiv: 2208.13640v3 [physics] (2022).

Description of included the papers

Manuscript [A] describes a proof of principles of the 0D-RATS method based on a rotary diffuser (attached as the first in annexes) - in the introductory part of the thesis as s Ref. [46]. Manuscript [B] shows the first implementation of 2D-RATS based on double diffused light and introduces the $FLIM_B$ reconstruction approach (attached as the second in annexes) - in the introductory part of the thesis as a Ref. [47]. An extensive noise analysis of the RATS method is performed in the manuscript [C] (attached as the third in annexes) - in the introductory part of the thesis as a Ref. [50]. Manuscript [D] presents a less time-consuming and less computationally intensive spectrogram reconstruction approach ($FLIM_A$) and points out the possibility of achieving a nanosecond timescale via the RATS method (attached as the fourth in annexes) - in the introductory part of the thesis as a Ref. [49].